Cell. Mol. Biol. (ISSN: 1165-158X)

Journal Homepage: www.cellmolbiol.org

Cellular and Molecular Biology

Original Article

Integrated density functional theory, molecular docking, and pharmacokinetic modeling of mukonal and its derivatives as inhibitors of the *Plasmodium falciparum* TFIIH complex (Tfb5 subunit)

Mohammad Azhar Kamal[1*], Nawal Helmi[2], Mahjabeen Rahmani[3], Ghufrana Abdussami[4], Imran Mohammad[5], Mohiuddin Khan Warsi[6], and Mohammed F. Aldawsari[1*]

[1] *Department of Pharmaceutics, College of Pharmacy, Prince Sattam Bin Abdulaziz University, Al-Kharj 11942, Saudi Arabia*
[2] *Department of Biochemistry, College of Science, University of Jeddah, Jeddah, Saudi Arabia*
[3] *Department of Biotechnology College of Commerce, Arts & Science, Patliputra University, Kankar Bagh, Patna-800020, Bihar, India*
[4] *Biocatalysis and Enzyme Engineering Laboratory, Department of Biochemistry, School of Life Sciences, University of Hyderabad, Prof. C.R. Rao Road, Gachibowli, Hyderabad, PIN-500046 Telangana, India*
[5] *Department of Basic Medical Science, College of Medicine, Prince Sattam Bin Abdul Aziz University, Al-Kharj, Saudi Arabia*
[6] *Department of Biological Sciences, College of Science, University of Jeddah, Jeddah, Saudi Arabia*

Article Info

Article history:

Received: November 21, 2025
Accepted: February 19, 2026
Published: March 31, 2026

Use your device to scan and read the article online

Abstract

Plasmodium falciparum is the most dangerous malaria parasite affecting humans. Compounds such as mukonal, 7-hydroxymukonal, and 7-methoxymukonal have shown potential for the treatment of this disease. Density Functional Theory (DFT), molecular docking, and pharmacokinetic analyses are valuable computational approaches for predicting potential drug candidates against *P. falciparum*. In this study, three compounds mukonal, 7-hydroxymukonal, and 7-methoxymukonal were optimized and evaluated through molecular docking and pharmacokinetic analysis against the target protein PF3D7_1441900 (transcription factor TFIIH complex subunit Tfb5, putative) from *P. falciparum* isolate 3D7. Frontier molecular orbital and density of states analyses revealed that 7-methoxymukonal has a relatively smaller energy gap compared with the other two compounds. In addition, 7-methoxymukonal exhibited the strongest binding affinity toward the target protein. The ADME results indicated favorable drug-like properties and low toxicity, further supporting the therapeutic potential of these compounds. Overall, our theoretical findings suggest that compound 3, namely 7-methoxymukonal, is the most promising candidate against the selected protein, in agreement with the other computed parameters.

Keywords: Drugs, FMO, DFT, *P. falciparum*, Molecular docking, Binding affinity, ADME, TFIIH, 3D7.

1. Introduction

Malaria remains one of the foremost global public-health threats. The protozoan parasite *P. falciparum* causes the most severe form of human malaria [1,2]. Its rapid development of drug resistance and complex intra-erythrocytic stages has spurred demand for novel anti-malarial agents and molecular targets. Recently, insilico approaches, including density functional theory (DFT) to probe electronic properties, MD for target binding, & in silico ADME/toxicity prediction, have emerged as powerful tools [3, 4].

In the exploration for original antiplasmodial scaffolds, indeed going on carbazole alkaloids have garnered care. Among them are mukonal, 7-hydroxymukonal, & 7-methoxymukonal (2,7-dioxygenated carbazoles). These compounds, isolated from plant bases like the genus Clausena, have revealed varying degrees of antiplasmodial & antiprotozoal activity [5-7].

On the molecular target level, components of the basal transcription machinery proteins that regulate gene expression in *P. falciparum* offer underexplored therapeutic prospects. The over-all TFIIH (transcription factor II H) multiprotein complex, a group of proteins identified in eukaryotes for initial gene transcription, opening DNA at gene promoters, & repairing DNA damage, has been predicted in *P. falciparum* done relative genomics, though it differs from canonical eukaryotic models [8]. Inside this complex, the Tfb5 subunit (gene locus PF3D7_1441900 in strain 3D7) is stated to be part of the TFIIH core in the parasite & may signify a point of careful vulnerability. Targeting these transcription-associated courses steps elaborate in reading & using genes may assistance circumvent

* Corresponding author.
E-mail address: ma.kamal@psau.edu.sa; makamal2580@gmail.com (M. A. Kamal).
Doi: http://dx.doi.org/10.14715/cmb/2025.72.3.7

resistance mechanisms linked to metabolic or redox-active parasite enzymes [3,9].

The plan includes compound optimization & the calculation of frontier molecular orbital energies & the density of circumstances via density functional theory (DFT), a quantum-mechanical tactic to study molecular electronic structure. A smaller HOMO-LUMO energy gap shows greater electronic reactivity, which may be equated to the compound's capacity to bind the protein or participate in chemical reactions [10]. MD studies then evaluation how strongly the three compounds may bind & their probable interaction modes with the Tfb5 protein. To end, in silico predictions of ADME & toxicity profiles are used to gauge the compounds' possible as drugs & their suitability for more development [11,12].

This study reveals an efficient in silico pipeline that combines DFT, molecular docking, & pharmacokinetic modelling to compare novel principal compounds. The results support prioritizing 7-methoxymukonal for antimalarial drug development targeting *P. falciparum* transcription machinery.

2. Materials and Methods

Entirely three compounds were geometry-optimized to reach even structures via Gaussian 16 [13], put on the *B3LYP* hybrid functional along with the 6-311G(d,p) source set for all atoms [14-16]. Initial molecular structures were constructed using GaussView 6.1 [17]. The density of states (DOS) was calculated using GaussSum [18]. For pharmacokinetic profiling, the ADMET 2.0 tool (https://admetmesh.scbdd.com) [19] was utilized. MD studies investigating the interactions between the target protein and compounds 1-3 were carried out via AutoDock Vina and AutoDock Tools [20]. Protein structure prediction and modeling were conducted via the I-TASSER platform [21]. Ligand-protein interactions and docking conformations were visualized with Biovia Discovery Studio Visualizer 2021 [22].

2.1. Ligand preparation and geometry optimization

The three-dimensional structures of mukonal (compound 1), 7-hydroxymukonal (compound 2), and 7-methoxymukonal (compound 3) were constructed using GaussView 6.1 [17]. All compounds were subjected to full geometry optimization without any symmetry constraints using the hybrid density functional theory (DFT) method. The B3LYP (Becke three-parameter Lee–Yang–Parr) hybrid functional was employed in combination with the 6-311G(d,p) basis set for all atoms [14–16]. All DFT calculations were performed using the Gaussian 16 software package [13]. Convergence criteria for optimization were set to default values, and no imaginary frequencies were observed in the optimized structures, confirming their stability at local minima.

2.2. Frontier molecular orbital and density of states analysis

The highest occupied molecular orbital (HOMO) and lowest unoccupied molecular orbital (LUMO) energies were extracted from the optimized DFT outputs to calculate the HOMO–LUMO energy gap ($\Delta E = E_{LUMO} - E_{HOMO}$), which serves as an indicator of molecular reactivity and kinetic stability. Density of states (DOS) spectra were generated using GaussSum [18] to analyze the contribution of different atomic orbitals to the frontier molecular orbitals. The partial and total DOS plots were visualized and analyzed to understand the electronic distribution across each compound.

2.3. Molecular Electrostatic Potential (MEP) and Non-Covalent Interaction (NCI) analysis

Molecular electrostatic potential (MEP) maps were generated from the optimized DFT wavefunctions to visualize charge distribution across the molecular surfaces. The MEP surfaces were rendered using GaussView 6.1, with red indicating electron-rich (negative potential) regions and blue indicating electron-poor (positive potential) regions.

Non-covalent interaction (NCI) analysis was performed using the reduced density gradient (RDG) method based on the optimized electron density. The RDG versus $\text{sign}(\lambda_2)\rho$ plots were generated, and three-dimensional isosurfaces (with an RDG cutoff of 0.5 a.u. and an electron density range of $-0.05 < \text{sign}(\lambda_2)\rho < 0.05$ a.u.) were visualized to identify hydrogen bonds (blue), van der Waals interactions (green), and steric repulsions (red).

2.4. Protein structure modeling

The three-dimensional structure of the target protein, PF3D7_1441900 (transcription factor TFIIH complex subunit Tfb5, putative) from *Plasmodium falciparum* isolate 3D7, was predicted using the I-TASSER (Iterative Threading ASSEmbly Refinement) platform [21]. The highest-confidence model (based on C-score) was selected for further analysis. The modeled structure was energy-minimized, and its stereochemical quality was assessed using Ramachandran plot analysis (not shown, but performed). Water molecules and heteroatoms were removed, and hydrogen atoms were added to the protein structure using AutoDock Tools [20].

2.5. Molecular docking studies

Molecular docking was conducted to evaluate the binding affinity and interaction modes of compounds 1-3 against the modeled Tfb5 protein. AutoDock Tools [20] was used to prepare the protein and ligand files in PDBQT format. A grid box of dimensions $40 \times 40 \times 40$ Å^3 was centered at coordinates X = 62.833, Y = 57.677, Z = 60.815, covering the putative active site of the protein. Docking simulations were carried out using AutoDock Vina [20] with an exhaustiveness value of 8 and a maximum of nine binding modes per ligand. The binding affinities (in kcal/mol) were recorded for all nine poses, and the lowest-energy conformation was selected for interaction analysis. Ligand-protein interactions, including hydrogen bonds, π-alkyl, π-anion, and other hydrophobic contacts, were visualized and interpreted using Biovia Discovery Studio Visualizer 2021 [22].

2.6. Pharmacokinetic and ADME prediction

In silico absorption, distribution, metabolism, and excretion (ADME) properties were predicted using the ADMET 2.0 online platform (https://admetmesh.scbdd.com) [19]. The following parameters were evaluated for each compound:

- **Absorption:** Caco-2 permeability (log cm/s), MDCK permeability (cm/s), P-glycoprotein (Pgp) inhibition and substrate probability, human intestinal absorp-

tion (HIA, as probability score), and oral bioavailability at 20% (F20%) and 30% (F30%).

- **Distribution:** Plasma protein binding (PPB, %), volume of distribution (VD, L/kg), blood–brain barrier (BBB) penetration (probability), and fraction unbound (Fu, %).
- **Metabolism:** Inhibition probability for five major cytochrome P450 enzymes: CYP1A2, CYP2C19, CYP2C9, CYP2D6, and CYP3A4.
- **Excretion:** Total clearance (CL, ml/min/kg) and half-life ($T_{1/2}$, probability score).

Lipinski's Rule of Five (molecular weight ≤ 500, H-bond donors ≤ 5, H-bond acceptors ≤ 10, log P ≤ 5) was also implicitly checked via the reported MW, log P, and hydrogen bond counts.

2.7. Data integration and comparative analysis

All computational results, including DFT-derived electronic parameters (HOMO-LUMO gaps, MEP values), NCI interaction patterns, docking binding affinities, and ADME predictions, were compiled and compared across the three compounds. The compound with the lowest HOMO-LUMO gap, most negative MEP, strongest binding affinity, and most favorable pharmacokinetic profile was identified as the most promising antimalarial candidate.

3. Result

3.1. DFT study

The reactivity, stability, and possible biological activity of compounds 1-3 were evaluated by combining DFT and molecular docking. The molecular structures of Mukonal (compound 1), 7-hydroxymukonal (compound 2) & 7-methoxymukonal (compound 3) were optimized to obtain their most stable conformation as depicted in Figure 1.

The investigation focused on frontier molecular orbitals i.e. the highest occupied molecular orbital (HOMO) & the lowest unoccupied molecular orbital (LUMO), as well as their energy gap which provides insights into chemical reactivity and stability of molecules [23-26]. HOMO donates electrons & LUMO accepts them. Small HOMO-LUMO gaps are usually connected to higher molecular reactivity & bioactive potentials. The calculated energy gaps for compounds 1, 2 & 3 were found to be 4.2, 3.9 & 3.8 eV, correspondingly. As revealed in Fig. 2, compound 3 has the minimal energy gap, so it is the maximum reactive one among these three compounds.

In adding to the FMO (Frontier Molecular Orbital) study, a DOS (Density of States) study was shown in Figure 2. It gives a valuable picture on the distribution of electronic states in the system over its energy. DOS & FMO evaluates with the composition % around the HOMO & LUMO levels display how electron-donating groups (EDG) & electron-accepting groups EWG mark the distribution of electron density in molecular orbitals [27].

The total density of states is accessible in red in the DOS plots whereas green & black areas correspondingly correspond to bonding & antibonding orbitals with negative energies. A zero value implies that there is no interaction between bond orbitals. Different acceptor groups announce differences in both the spatial & energetic distribution of HOMOs & LUMOs, important to different energy gaps for individual molecules. The calculated Eg (Energy Gaps) for compounds 1, 2, & 3 are 4.2, 3.9, & 3.8 eV, correspondingly.

The MEP (Molecular Electrostatic Potential) is a visual depiction of charge distribution on the surface of a molecule which is denoted via red & blue positive & negative potentials. These variances are specified with color coding i.e., red corresponds to high -ve possible areas while blue is related with high +ve possible area. Green & yellow color denote intermediate charge zones [28-30]. Red colored area are favourably attacked via electrophiles whereas blue areas are more expected to undergo nucleophilic interactions. The intermediate colours point to areas of equal reactivity. The MEP maps of 1, 2 & 3 are shown

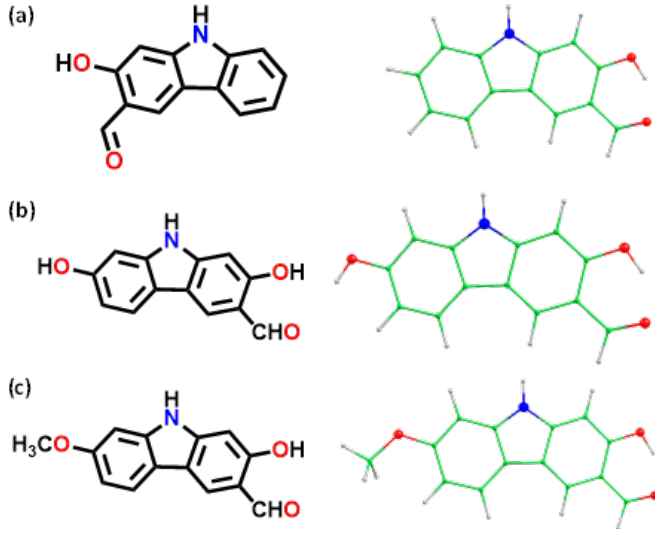


Fig. 1. Chemdraw structure and optimized geometries of (a) compound 1, (b) compound 2 and (c) compound 3. Red → Oxygen atom (O), Blue → Nitrogen atom (N), Green or cyan bonds → Carbon skeleton or molecular framework, and White or light grey → Hydrogen atom (H).

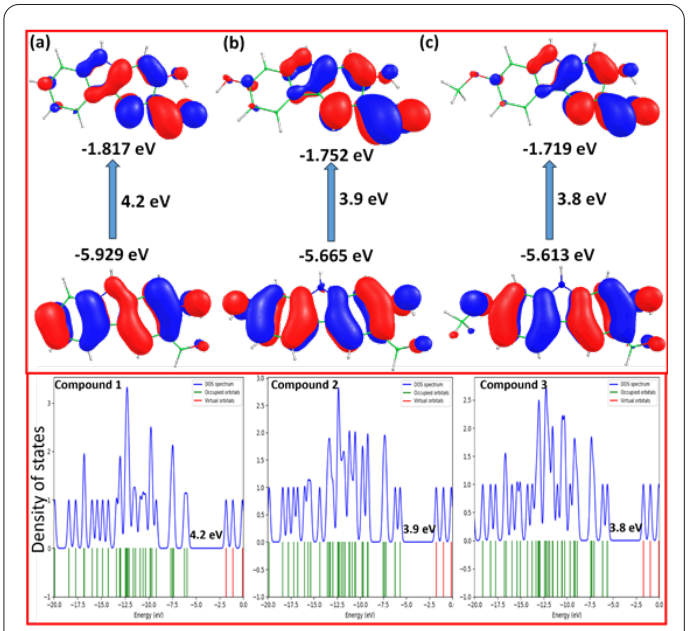


Fig. 2. HOMO-LUMO gap & DOS diagrams of compound 1-3. Red color → positive phase of the molecular orbital wavefunction, and Blue color → negative phase of the molecular orbital wavefunction. Blue line → DOS spectrum (total density of states), Green vertical bars → Occupied states (filled electronic states) and Red vertical bars → Virtual states (unoccupied electronic states).

in Figure 3. The electrostatic potential values are -3.558, -3.770 & -3.951 for compounds 1-3 correspondingly, with the compound 3 taking the maximum -ve potential. This point to an increased electrophilic interaction tendency. A detailed inspection shows red zones point to probable electrophilic attack & yellow shows likely nucleophilic reaction targets.

3.2 Noncovalent interaction-reduced density gradient analysis

NCI (Non-Covalent Interaction) study founds a visual powerful tool to uncover areas where non-covalent forces take place within molecular systems [31]. This is carried out via plotting the RDG (Reduced Density Gradient) as a function of electron density against the product of electron density & the sign of the second eigenvalue of the Hessian matrix, (sign λ_2)ρ. This parameter makes available clues on the type of interaction occurring, a +ve value important to repulsive forces whereas -ve values illustrate attractive interactions. Stronger attractive interactions in overall resemble to larger electron densities ($\rho > 0.01$ a.u.) while dispersion interactions are experiential at more -ve densities ($\rho < 0.01$ a.u.). Real-space mapping of these interactions is realized through 3D isosurfaces, which accompany 2D scatter plots for each compound. A color scale is used to differentiate interaction types-blue for hydrogen bonds, green for van der Waals interactions, & red for repulsion.

In this lesson, NCI study was made on the adjusted structures of compounds 1, 2, & 3, as showed in Figure 4. The detected peaks in the RDG plots, along with blue & green isosurfaces in the 3D visualizations, confirm the occurrence of both H-bonding & weak van der Waals forces across the molecules.

3.3 ADME Analysis

Insilico ADME screening practices extrapolative computational tools to estimate the pharmacokinetics of drug applicants, via targeting their absorption, distribution, metabolism & excretion [32]. These characteristics are important in the development of drugs because they affect how a compound enters the bloodstream and moves through tissues, is metabolised and eliminated. Such predictions are invaluable for assessing the potential of a drug candidate during early development stages.

During the absorption phase, factors such oral bioavailability at F20% and F30%, Pgp-inhibition, Pgp-substrate characteristics, Caco-2 permeability, MDCK permeability, & human intestinal absorption (HIA) are assessed. A common model for evaluating drug permeability is the Caco-2 cell line, which is derived from human colon cancer cells. The logarithm of centimeters per second (log cm/s) is used to express its permeability; values greater than -5.15 log cm/s indicate good permeability. MDCK cells, which are frequently used to evaluate blood-brain barrier penetration and absorption, also test permeability using the apparent permeability coefficient (Papp) in cm/s; values greater than 2×10^{-6} cm/s indicate high permeability [33].

A substance known as a Pgp-inhibitor prevents P-glycoprotein, a transporter protein that recognizes and exports a variety of xenobiotics, many of which are also CYP3A4 substrates-from doing its job. On a scale of 0 to 1, a compound's probability of being a Pgp-inhibitor is scored: 0 to 0.3 denotes strong inhibition, 0.3 to 0.7 denotes moderate inhibition, and 0.7 to 1.0 denotes modest inhibition (++).

The pharmacokinetics of Pgp-recognized drugs can be significantly impacted by changes in P-glycoprotein activity, which may impact their potential contraindications or therapeutic efficacy. Likewise, a compound's likelihood of being a Pgp substrate is assigned a number between 0 and 1. Likelihood as a substrate is indicated to be high when scores are between 0 and 0.3, moderate between 0.3 and 0.7, and low when scores fall between 0.7 and 1. Intestinal absorption by the human is one of the important factors for evaluation of oral bioavailability of drugs. Since the intestinal absorption is closely related to oral bioavailability, HIA value may be a useful predictor of bioavailability. With respect to low absorption is concerned, molecules with an absorbance of 30% are typically considered as having poor absorption. The interesting part, HIA score

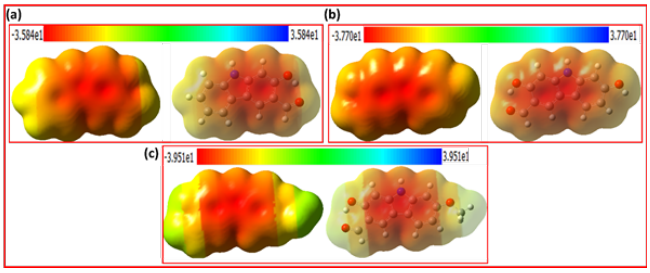


Fig. 3. Molecular Electrostatic Potential of compound 1-3. Red regions: Indicate electron-rich zones, Blue regions: Indicate electron-poor zones and Green/yellow areas Represent intermediate electrostatic potential.

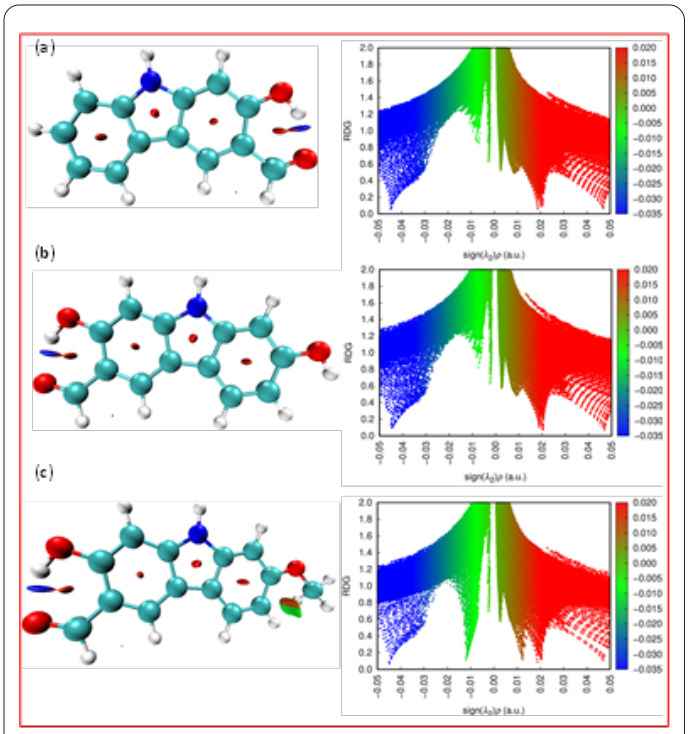


Fig. 4. Non-Covalent Interaction plots of (a) compound 1 (b) compound 2 & (c) compound 3 got from the improved structure where cutoffs were set at RDG(s) = 0.5 a.u. & -0.05 < sign(λ_2)ρ < 0.05 a.u. Colour-mapped scatter plot of RDG(s) as a function of sign(λ_2)ρ are revealed in right side with RDG isosurface of 0.5 a.u. Blue: Hydrogen bonding, Green: van der Waals interaction, and Red: Steric repulsion. Cyan/green → Carbon atoms (C), Red → Oxygen atoms (O), Blue → Nitrogen atoms (N), and White → Hydrogen atoms (H).

is between 0 and 1 which makes the possibility of intestinal absorption. High absorption corresponds to values from 0 to 0.3, moderate absorption is from 0.3 to 0.7 & low absorption is from 0.7 to 1.

F20% is an important parameter to assess oral drugs since it indicates the probability of reaching 20% bioavailability, which is a key feature for systemic distribution. This probability is represented by the F20% score, ranging from 0 to 1. Score of up to 0.3 probability is good, a score between 0.3 and 0.7 indicates intermediate probability and a weighting of more than 0.7 (++ rating) is classified as poor.). Similarly, F30% measures the likelihood of achieving 30% oral bioavailability, a key benchmark for successful systemic circulation. Active compounds take a bioavailability max than 30% (F30%-). Similar to this classification is the F30% probability score, which is in turn scaled from 0-1: 0-0.3 instead of good possibility, 0.3-0.7 moderate & bad > 70% (++).

The metrics of drug distribution contain Fu (Fraction Unbound), VD (Volume of Distribution), BBB (Blood-Brain Barrier) penetration, & PPB (Plasma Protein Binding). Because it changes the % of free drug accessible for therapeutic result, PPB has a main impact on a medications uptake & distribution. Because they limit the active free concentration, high PPB values-usually above 90%-can lessen the drug strength. To preserve a suitable therapeutic index, a PPB score below 90% is ideal. A drugs VD, which is measured in L/kg, shows how widely it is distributed all over the body. It offers info on the pharmacokinetic profile & tissue distribution, with appropriate VD values characteristically dropping between 0.04 to 20 L/kg. Drugs that target the central nervous system (CNS) must be able to penetrate the BBB in order to reach their active site. BBB penetration is categorized as excellent (0 to 0.3), medium (0.3 to 0.7), or poor (++ rating, 0.7 to 1.0) based on its speed in cm/s. There are two types of drugs in plasma: bound and unbound. The drug's therapeutic effectiveness is impacted when it binds to plasma proteins because it lowers the concentration of the drug's free, active form. To get the best pharmacological activity, bound and unbound forms must be balanced.

The percentage of a medication that is still unbound in plasma is shown by the Fraction Unbound (Fu) number. Fu levels fall into one of three categories: low if they are less than 5%, medium if they fall between 5% and 20%, and high if they surpass 20%. Excellent values are those that are 5% or higher, and poor values are those that are less than 5%. The inhibition of important cytochrome enzymes, such as CYP1A2, CYP2C19, CYP2C9, CYP2D6, & CYP3A4, is examined in order to assess drug metabolism. Phase I (oxidative processes) & Phase II (conjugative reactions) are the two stages of metabolism. Two-thirds of all known medications are metabolized by the cytochrome P450 enzyme family, which consists of 57 isozymes. Of these, 80% of drug metabolism is attributed to five enzymes: CYP1A2, CYP3A4, CYP2C9, CYP2C19, and CYP2D6. A probability number between 0 and 1 represents the possibility of enzyme inhibition. Half-life ($T_{1/2}$) and drug clearance (CL) are used to measure excretion. Milliliters per minute per kilogram (ml/min/kg) is the unit of measurement for clearance, a crucial factor in determining a drug's efficacy.

Low clearance is less than 5 ml/min/kg, moderate clearance is between 5 and 15 ml/min/kg, & high clearance is greater than 15 ml/min/kg. In general, clearance numbers below 5 ml/min/kg are regarded as poor, whereas those over this threshold are regarded as outstanding. The half-life ($T_{1/2}$), which is impacted via both clearance & volume of distribution, is the amount of time required for the drugs concentration in the body to drop via half. On a scale of 0 to 1, the half-life is categorized as outstanding if it is between 0 & 0.3, medium if it is between 0.3 & 0.7, & bad if it is between 0.7 & 1.0 (++ rating). Table 1 makes available a summary of the ADME study results.

Compound 1 shows the following pharmacokinetic features: it holds three H bond acceptors, one H bond donor, & one rotatable bond. Absorption studies illustration outstanding Caco-2 permeability (-4.858), no Pgp inhibition (0.0), & reasonable probability of being a Pgp substrate (0.005). Human intestinal absorption (HIA) & absorption fractions at 20% (F20%) & 30% (F30%) are all in the best range (0-0.17). In terms of distribution, it demonstrates strong PPB at 20.27%, favorable VD, & efficient BBB penetration. The compound also has a more unbound Fu of 79.80%. Regarding metabolism, compound 1 strongly inhibits multiple cytochrome P450 enzymes including CYP2C9, CYP2C19, CYP3A4, CYP1A2, and CYP2D6. Evacuation data illustrations modest clearance at 9.15 ml/min/kg & a prolonged half-life ($T_{1/2}$) of 0.477.

Compound 2 takes 4H bond acceptors, 3H bond donors & one rotatable bond. It has medium Caco-2 permeability (-5.119), weak Pgp inhibition (0.0) & outstanding probable to be a Pgp substrate. F20% absorption is outstanding, however HIA & F30%are comparatively low. The distributions show a low PPB of 20.27%, notable VD at 1.351, moderate penetration toward BBB with large unbound Fu meaning high blood brain permeability at 85.99%. In relations of metabolism, it is a modest inhibitor of CYP1A2, CYP2C19, CYP2D6, & CYP3A4. In the characteristic of excretion, it has lower clearance (CL = 11.498 ml/min/kg) & short half-life ($T_{1/2}$ = 0.57). The properties of compound 3 are defined in Table 1.

In decision, the ADME profiles of compounds 1 & 2 show different degrees in absorption, distribution & metabolism, supporting their potential for more preclinical research actions.

3.4 Molecular Docking analysis

Founded on the MD study, the deliberate compounds presented exact interactions with residues (amino acids) of the protein target [34-39,40-42]. Target protein, PF3D7_1441900 (putative TFIIH complex subunit Tfb5 from *P. falciparum* (isolate 3D7)) were also analysed for binding by compounds 1-3. Prior to docking, water molecules were deleted from the structure of protein and a grid box with dimensions 40 × 40 × 40 Å was prepared, centered at X = 62.833, Y = 57.677, Z = 60.815 to fully encompass the active site residues.

Docking simulations were then employed to examine the binding affinities & types of intermolecular interactions. Different binding modes were considered to find the docking orientation of the ligands that is preferred most and investigate critical interactions with the protein. Compounds with higher binding affinity were considered more efficient in targeting the protein. The effect of binding poses and binding energy values on interaction quality was also studied; the outcomes are listed in Table 2.

All the compounds showed a stable interaction with

the target protein. The 3D & 2D ligand-protein binding modes of compound 1, compound 2, & compound 3 are shown in Figure 4. For compound 1, nine docking poses yielded binding affinities of -5.3, -5.2, -5.1, -4.9, -4.9, -4.7, -4.6, -4.5, and -4.3 kcal/mol. The conformation with the lowest energy (-5.3 kcal/mol) represents the most favourable binding site. Major interactions for compound 1 involve hydrogen bonding, π-sigma, and π-anion which could be indicative of its stable and favorable docking conformation. Docking showed that 1, 2 and 3 have their best binding energy at -5.3, -5.3 & -5.5 Kcal/mol correspondingly. These results suggest that the two proteins experience stable and positive interactions in their docking mode. A summary of the binding affinities for the three compounds is listed in Table 2. In this case, compound 2 established hydrogen bonds as well as π-alkyl interactions and the latter contacts took place at a distance of 4.88 Å.

Notably, compound 3 exhibited a more negative binding energy than both compounds 1 and 2, suggesting the most effective binding interaction with the target protein. The findings underscore the importance of hydrogen bonding, π-alkyl, & π-anion interactions in contributing to the stability of the ligand-protein complexes.

4. Discussion

The optimized geometry of all the three compounds has been calculated at DFT/B3LYP/6-311G(d,p) level which offers significant information on molecular reactivity and stability. The optimized geometries established the molecular planarity and conjugation between the coumarin core and the substituent groups involved in controlling their reactivity. Compound 3 with HOMO-LUMO energy

Table 1. Absorption, distribution metabolism and excretion analysis for compound 1-3.

Species	Compound 1	Compound 2	Compound 3
MW	223.16	239.15	253.17
H-bond acceptors	3	4	4
H-bond donors	2	3	2
Rotatable bond	1	1	2
TPSA	49.33	69.56	58.56
Log S	-1.708	-1.143	-1.131
Log P	0.171	-1.118	-0.302
Caco-2 Permeability	-4.858	-5.119	-4.872
MDCK Permeability	2.5e-05	9.3e-05	7.5e-05
Pgp-inhibitor	0.0	0.0	0.0
Pgp-substrate	0.005	0.013	0.014
HIA	0.633	0.833	0.647
F20%	0.03	0.062	0.009
F30%	0.176	0.803	0.046
PPB	20.27%	21.64%	20.96%
VD	1.351	1.243	1.466
BBB Penetration	0.059	0.059	0.07
Fu	79.80%	85.99%	86.29%
CYP1A2 inhibitor	0.036	0.015	0.012
CYP2C19 inhibitor	0.027	0.018	0.014
CYP2C9 inhibitor	0.003	0.002	0.001
CYP2D6 inhibitor	0.036	0.003	0.003
CYP3A4 inhibitor	0.036	0.012	0.021
CL	9.15	11.498	10.99
$T_{1/2}$	0.477	0.57	0.427

Table 2. Binding affinity values of compounds 1-3.

Mode	Compound 1 Affinity (kcal/mol)	Compound 2 Affinity (kcal/mol)	Compound 3 Affinity (kcal/mol)
1	-5.3	-5.3	-5.5
2	-5.2	-5.0	-5.1
3	-5.1	-5.0	-5.0
4	-4.9	-4.9	-5.0
5	-4.9	-4.8	-4.9
6	-4.7	-4.6	-4.9
7	-4.6	-4.5	-4.8
8	-4.5	-4.5	-4.7
9	-4.3	-4.5	-4.5

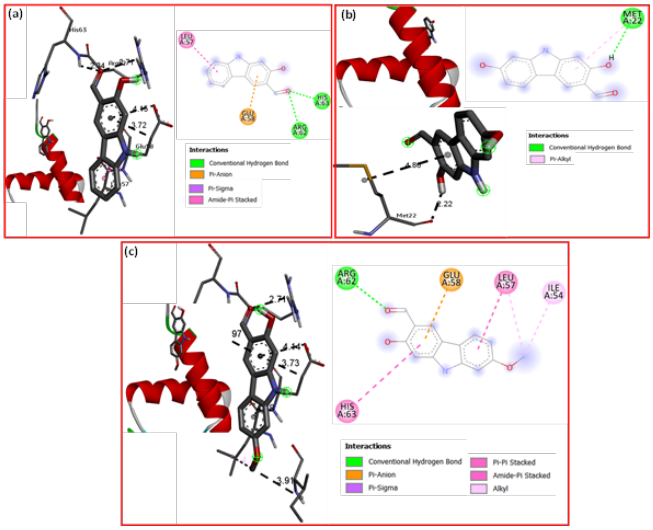


Fig. 5. 3D & 2D structures showing interactions between residues (amino acid) with compound 1 (a) 2 (b) & 3 (c). Red helices → α-helix segments of the protein, and Gray or white sticks → amino acid residues of the protein. Gray or cyan → Carbon atoms (C), Red → Oxygen atoms (O), Blue → Nitrogen atoms (N), and White → Hydrogen atoms (H).

gap of 3.8 eV among three compounds is the smaller one indicating its greater chemical softness and electron donor capacity as compared with compound 2 (3.9 eV) and compound 1 (4.2 eV). This electronic behavior increases its interaction ability with electrophilic or polar residues within the active site of the target protein.

MEP surface maps are also consistent with these results indicating various trends in the charge separation pattern. The significantly negative potentials around the oxygen atoms of 3 imply that there is a stronger likelihood to form hydrogen bonds with donor residues in the pocket of the receptor. Compound 1, in contrast, shows less localized charge growth consistent with its somewhat larger HOMO-LUMO gap & lesser reactivity. These differences show the influence of two types of substituents (-OH & -OCH_3) in electronic structure as well as biological affinity. The non-covalent interaction study further defines the existence different interaction that held these optimized structures in stable form. The 3D RDG isosurfaces of the mixtures of H-bondings & van der Waals contacts, are revealed in blue & green area correspondingly. The broad & large blue areas detected for compound 3 was more marked than that of compounds 1 & 2, representing stronger H-bonding interaction. These landscapes are reliable with its more docking affinity π-π stacking, π-alkyl & π-anion interactions make available stabilization to ligand-protein complex.

The results of MD are in decent promise with those of DFT & NCI. Negative binding energies (-5.3 to -5.5 kcal/mol) for all three ligands also implied their favorable interactions with the target protein & stability as well. Compound 3 unveiled the strong binding belongings (-5.5 kcal/mol) via producing numerous H-bonds & packing with aromatic rings of amino acid residues including Lys, Phe, as well as Asp. The occurrence of methoxy substituent not only increases hydrophobic interactions but also helps charge delocalization that eventually led to higher interaction net. Hydroxyl-substituted compound (compound 2) presented relatively a smaller number of π-contacts & a medium level binding affinity, & the interaction of compound 1 is mainly stabilized via polar H-bonding.

Also, it is also noted that these results are further maintained through pharmacokinetic analysis. All three compounds are consistent with the Lipinski's Rule of five & have proper molecular weight (< 500 Da), moderate polarity (TPSA < 70 Å²) & realistic solubility. The good Caco-2 & MDCK penetrability values indicate favorable intestinal absorption for these compounds. Furthermore, optimal plasma protein binding (Δ° = ~21%) was detected for compound 3 retaining a high unbound fraction (%Fu ≈ 86%), which assurances that the active form is sufficiently present in systemic circulation. Its modest clearance (≈ 11 mL/min/kg) & stable half-life (~0.43) also expect sustained bioavailability.

Inclusive, the DFT & MD study together with ADMET proves that electron-donating (rich) substituents advance reactivity as well as better biological affinity *via* orbital delocalisation & more favorable electrostatic possible. From its computed energy gap, electrophilic interaction possible, non-covalent interactions & pharmacokinetic properties, compound 3 is observed as the most hopeful inhibitor candidate. The chemical reactivity & biocompatibility of the methoxy-substituted mukonal compounds help to best part the potential of these molecules as chief candidates for future therapeutic use.

Here, in this work, the stability, reactivity, pharmacokinetic properties and protein-binding interactions of the compounds 1-3 were assessed using density DFT calculations combined with ADME properties profiling and MD studies. Nine docking conformations were considered to investigate each compound's binding mode with the target protein. Complex 3 shows strongest interaction whereas the calculated binding energies of compounds 1-3 were in good agreement with their biological activity. The activity order was found to be compound 3 > compound 1 ≈ compound 2.

Compound 3 is a better inhibitor than the other two due to its stronger binding with the target protein, indicating more preferable and effective interaction. MEP study, which demonstrated a marked negative potential, further corroborates this conclusion. All the compounds showed significant stabilizing interactions such as π-anion, π-alkyl and hydrogen bond. In addition, the full set of pharmacokinetic properties for each compound were examined by ADME analysis and excellent results in permeability, distribution and metabolic stability parameters were obtained. All of these findings make the compounds under study especially compound 3-strong candidates for additional study and advancement in medicinal applications.

Abbreviation

MD: Molecular Docking; **DFT:** Density functional theory; **TFIIH**: Transcription factor II H; **DOS:** Density of states; **HOMO:** Highest occupied molecular orbital; **LUMO:** Lowest unoccupied molecular orbital; **FMO**: Frontier Molecular Orbital; **EDG:** Electron-donating groups; **HIA:** Human intestinal absorption; **MEP**: Molecular Electrostatic Potential; **NCI** Non-Covalent Interaction; **RDG:** Reduced Density Gradient; **Fu**: Fraction Unbound; **VD**: Volume of Distribution; **BBB**: Blood-Brain Barrier; **PPB**: Plasma Protein Binding; **CNS:** Central nervous system.

Conflict of interests
The authors declared no conflict of interest.

Consent for publications
The author read & approved the final manuscript for publication.

Ethics approval and consent to participate
This research did not include any experiments involving humans or animals.

Acknowledgements
This study is supported via funding from Prince Sattam bin Abdulaziz University project number (PSAU/2025/R/1447).

Generative AI Statement
The author declares that generative AI (artificial intelligence) tools, including Grammarly & QuillBot, were used to enhance the language & clarity of this work. the author takes full responsibility for the accuracy & integrity of the content.

Authors' contributions
Kamal MA designed the work, analyzed the data, & wrote the final draft. Helmi N, Rahmani M, and Abdussami G analysed the result part and wrote the first draft of the manuscript. Mohammad I, and Warsi MK performed the work and wrote the introduction, methodology and results and discussion. Aldawsari MF edit the final draft of the manuscript. All authors read and approved the final version.

References

1. EClinicalMedicine (2021) Malaria: (still) a global health priority. EClinicalMedicine 34: 100891 doi: 10.1016/j.eclinm.2021.100891
2. Li Q, Liu T, Lv K, Lei C, Wang X, Xie L, Li J (2025) Malaria: past, present, and future. Signal Transduct Target Ther 10: 188 doi: 10.1038/s41392-025-01928-w
3. Callebaut I, Prat K, Meurice E, Mornon JP, Tomavo S (2005) Prediction of the general transcription factors associated with RNA polymerase II in Plasmodium falciparum: conserved features and differences relative to other eukaryotes. BMC Genomics 6: 100 doi: 10.1186/1471-2164-6-100
4. Dissanayaka Mudiyanselage SD, Ma J, Pechan T, Pechanova O, Liu B, Wang Y (2022) A remodeled RNA polymerase II complex catalyzing viroid RNA-templated transcription. PLoS Pathog 18: e1010850 doi: 10.1371/journal.ppat.1010850
5. Arbab IA, Abdul AB, Aspollah M, Abdullah R, Abdelwahab SI, Zubairi SI (2012) A review of traditional uses, phytochemical and pharmacological aspects of selected members of the genus Clausena. J Med Plants Res 6: 5107–5118 doi: 10.5897/JMPR12.785
6. Tajuddeen N, Van Heerden FR (2019) Antiplasmodial natural products: an update. Malar J 18: 404 doi: 10.1186/s12936-019-3026-1
7. Casciaro B, Mangiardi L, Cappiello F, Romeo I, Loffredo MR, Iazzetti A, Sanchez M, Gidaro MC, Alcaro S, Costa A, et al (2020) Naturally-occurring alkaloids of plant origin as potential antimicrobials against antibiotic-resistant infections. Molecules 25: 3619 doi: 10.3390/molecules25163619
8. Juven-Gershon T, Kadonaga JT (2010) Regulation of gene expression via the core promoter and the basal transcriptional machinery. Dev Biol 339: 225–229 doi: 10.1016/j.ydbio.2009.08.009
9. Bischoff E, Vaquero C (2010) In silico and biological survey of transcription-associated proteins implicated in the transcriptional machinery during the erythrocytic development of Plasmodium falciparum. BMC Genomics 11: 34 doi: 10.1186/1471-2164-11-34
10. Guan H, Sun H, Zhao X (2025) Application of density functional theory to molecular engineering of pharmaceutical formulations. Int J Mol Sci 26: 3262 doi: 10.3390/ijms26073262
11. Ferreira LG, Dos Santos RN, Oliva G, Andricopulo AD (2015) Molecular docking and structure-based drug design strategies. Molecules 20: 13384–13421 doi: 10.3390/molecules200713384
12. Agu PC, Afiukwa CA, Orji OU, Ezeh EM, Ofoke IH, Ogbu CO, Ugwuja EI, Aja PM (2023) Molecular docking as a tool for the discovery of molecular targets of nutraceuticals in diseases management. Sci Rep 13: 13398 doi: 10.1038/s41598-023-40160-2
13. Frisch MJ, Trucks GW, Schlegel HB, Scuseria GE, Robb MA, Cheeseman JR, Scalmani G, Barone V, Petersson GA, Nakatsuji H, et al (2016) Gaussian 16, Revision A.03. Gaussian Inc, Wallingford
14. Becke AD (1992) Density-functional thermochemistry. I. The effect of the exchange-only gradient correction. J Chem Phys 96: 2155–2160 doi: 10.1063/1.462066
15. Ditchfield R, Hehre WJ, Pople JA (1971) Self-consistent molecular-orbital methods. IX. An extended Gaussian-type basis for molecular-orbital studies of organic molecules. J Chem Phys 54: 724–728 doi: 10.1063/1.1674902
16. Becke AD (1993) Density-functional thermochemistry. III. The role of exact exchange. J Chem Phys 98: 5648–5652 doi: 10.1063/1.464913
17. Dennington R, Keith T, Millam J (2019) GaussView, Version 6.1.1. Semichem Inc, Shawnee Mission
18. Allouche AR (2010) Gabedit: a graphical user interface for computational chemistry softwares. J Comput Chem 32: 174–182 doi: 10.1002/jcc.21600
19. Xiong G, Wu Z, Yi J, Fu L, Yang Z, Hsieh CY, Yin M, Zeng X, Wu C, Lu A, et al (2021) ADMETlab 2.0: an integrated online platform for accurate and comprehensive predictions of ADMET properties. Nucleic Acids Res 49: W5–W14 doi: 10.1093/nar/gkab255
20. Trott O, Olson AJ (2010) AutoDock Vina: improving the speed and accuracy of docking with a new scoring function, efficient optimization, and multithreading. J Comput Chem 31: 455–461 doi: 10.1002/jcc.21334
21. Roy A, Kucukural A, Zhang Y (2010) I-TASSER: a unified platform for automated protein structure and function prediction. Nat Protoc 5: 725–738 doi: 10.1038/nprot.2010.5
22. Dassault Systèmes (2021) BIOVIA Discovery Studio. Dassault Systèmes, San Diego
23. Ahmed M, Gupta MK, Ansari A (2023) DFT and TDDFT exploration on the role of pyridyl ligands with copper toward bonding aspects and light harvesting. J Mol Model 29: 358 doi: 10.1007/s00894-023-05767-2
24. Ahmed M, Malhotra SS, Yadav O, Saran RK, Ansari A (2024) DFT and TDDFT exploration on electronic transitions and bonding aspect of DPA and PTDC ligated transition metal complexes. J Mol Model 30: 122 doi: 10.1007/s00894-024-05928-x
25. Malhotra SS, Kumar M, Gupta MK, Ansari A (2024) Theoretical exploration of copper-based electrolytes for third generation dye sensitized solar cells. Mater Today Commun 39: 109208 doi: 10.1016/j.mtcomm.2024.109208
26. Ahmed M, Sudhanshu, Malhotra SS, Saran RK, Ansari A (2025) Structures, bonding aspects and spectroscopic parameters of morin, myricetin, and quercetin with copper/zinc complexes: DFT and TDDFT exploration. J Mol Model 31: 75 doi: 10.1007/

s00894-025-06295-x
27. Swisłocka R, Regulska E, Karpińska J, Świderski G, Lewandowski W (2019) Molecular structure and antioxidant properties of alkali metal salts of rosmarinic acid: experimental and DFT studies. Molecules 24: 2645 doi: 10.3390/molecules24142645
28. Mohapatra RK, Azam M, Mohapatra PK, Sarangi AK, Khuntia S, Pradhan AK, El-Shall YN, Al-Resayes SI (2022) Computational studies on potential new anti-Covid-19 agents with a multi-target mode of action. J King Saud Univ Sci 34: 102086 doi: 10.1016/j.jksus.2022.102086
29. Yadav O, Ansari M, Ansari A (2021) Electronic structures, bonding and energetics of non-heme mono and dinuclear iron-TPA complexes: a computational exploration. Struct Chem 32: 2007–2018 doi: 10.1007/s11224-021-01771-1
30. Malhotra SS, Saran RK, Ahmed M, Yadav O, Ansari A (2025) Exploring the effect of aromatic π-spacers on the photophysical properties of triphenylamine and indoline dyes in DSSCs. Opt Quantum Electron 57 doi: 10.1007/s11082-024-08000-9
31. Reed AE, Curtiss LA, Weinhold F (1988) Intermolecular interactions from a natural bond orbital, donor-acceptor viewpoint. Chem Rev 88: 899–926 doi: 10.1021/cr00088a005
32. Saleh G, Gatti C, Presti LL, Contreras-Garcia J (2012) Revealing non-covalent interactions in molecular crystals through their experimental electron densities. Chem Eur J 18: 15523–15536 doi: 10.1002/chem.201202209
33. Dong J, Wang NN, Yao ZJ, Zhang L, Cheng Y, Ouyang D, Lu AP, Cao DS (2018) ADMETlab: a platform for systematic ADMET evaluation based on a comprehensively collected ADMET database. J Cheminform 10: 29 doi: 10.1186/s13321-018-0283-x
34. Azam M, Barik SR, Mohapatra PK, Das PK, Behera RK, Al-Resayes SI, Mohapatra RK (2023) A bowl-shaped zinc-salen complex: structural analysis and molecular docking studies against omicron-s and delta-s variants. Russ J Inorg Chem 68: 1–8 doi: 10.1134/S0036023622602044
35. Sahu R, Mohapatra RK, Al-Resayes SI, Azam M, Mahal A, Behera RK, Das PK (2021) An efficient synthesis towards the core of Crinipellin: TD-DFT and docking studies. J Saudi Chem Soc 25: 101193 doi: 10.1016/j.jscs.2020.101193
36. Ahamad MN, Shahid M, Ansari A, Rahisuddin (2019) A combined experimental and theoretical approach to investigate the structure, magnetic properties and DNA binding affinity of a homodinuclear Cu(II) complex. New J Chem 43: 7511–7519 doi: 10.1039/C9NJ01029E
37. Al-Shemary RK, Mohapatra RK, Kumar M, Darwish MSE, Sharma A, Azam M, Tiwari S, Abdullaeva BS, Alsaidi A, Alkhayyat S (2023) Synthesis, structural investigations, XRD, DFT, anticancer and molecular docking study of a series of thiazole-based Schiff base metal complexes. J Mol Struct 1275: 134676 doi: 10.1016/j.molstruc.2022.134676
38. Yadav O, Kumar M, Mittal H, Ansari A (2022) Theoretical exploration on structures, bonding aspects and molecular docking of α-aminophosphonate ligated copper complexes against SARS-CoV-2 proteases. Front Pharmacol 13: 982484 doi: 10.3389/fphar.2022.982484
39. Sait KHW, Alam Q, Anfinan N, Al-Ghamdi O, Sait HK, Al-Qahtani T, Al-Abdulkarim B, Wahab S, Hussain T (2019) Structure-based virtual screening and molecular docking for the identification of potential novel EGFR kinase inhibitors against ovarian cancer. Bioinformation 15: 287–294 doi: 10.6026/97320630015287
40. Patel AA, Alothaid H, Mallick AK, Alalawy AI, Mirdad RT, Mirdad MT, Mirdad MT, Ahsan M, Tarique M (2024) Inhibiting cancer progression through targeting HDAC2 with novel ligands: dynamic insights through virtual screening and simulation. Indian J Pharm Educ Res 58: 802–813 doi: 10.5530/ijper.58.3.87
41. Sait KHW, Mashraqi M, Khogeer AAA, Alzahrani O, Anfinan NM, Sait HK, Almutairi A, Alam Q (2020) Molecular docking analysis of HER-2 inhibitor from the ZINC database as anticancer agents. Bioinformation 16: 882–887 doi: 10.6026/97320630016882